BOX TRUSS ANTENNA TECHNOLOGY STATUS*

J. V. Coyner and
E. E. Bachtell
Martin Marietta Denver Aerospace
Denver, Colorado

*Abstract appears in NASA CP-2447, Part 1, 1986, pp. 145-148.

BOX TRUSS ANTENNA DEVELOPMENT

This paper summarizes recent technology development activities for box truss structures and box truss antennas. Three primary activities will be reported: the development of an integrated analysis system for box truss mesh antennas; dynamic testing to characterize the effect of joint freeplay on the dynamic behavior of box truss structures; and the fabrication of a 4.5-meter diameter offset fed mesh reflector integrated to an all graphite-epoxy box truss cube (fig. 1).

- ANALYSIS OF BOX TRUSS MESH ANTENNAS
- DYNAMIC TESTING OF BOX TRUSS SPACE STRUCTURE
- FABRICATION OF 4.5M BOX TRUSS ANTENNA

Figure 1

HISTORY OF BOX TRUSS

Each year significant steps were taken in the maturity of the box truss design and the understanding of the supporting analysis. Figure 2 summarizes the evolution of the deployable box truss and related technology activities. During 1977 and 1978, the emphasis was placed on design and analytical verification of the box truss structure performance. During 1979, 1980, and 1981, design refinements and hardware fabrication were directed towards GFRP integration with primary emphasis on low cost. This activity culminated in the fabrication and demonstration of the 4.5-meter cube. During 1982, a full-scale prototype of a gate frame truss was fabricated and tested. Also, a mesh test model was fabricated to validate the mesh reflector analytical tools and to demonstrate fabrication techniques. During 1983 and 1984, mesh analytical work continued, metal matrix composite development made significant progress, precision joint designs were fabricated and demonstrated, and passive damping augmentation concepts were developed. During 1985 and 1986 a 4.5-meter mesh reflector was fabricated and dynamic testing of a 20 meter truss was performed.

1977 - BOX TRUSS DESIGN CONCEIVED ON IR&D
- DESIGN DEVELOPED AND ANALYZED ON "ON ORBIT ASSEMBLY" PROGRAM
- SINGLE FRAME DEMONSTRATION MODEL FABRICATED

1978 - DESIGN AND FABRICATION OF SINGLE FRAME PROTOTYPE STRUCTURE (GFRP TUBES AND METALLIC FITTINGS)

1979 - DESIGN REFINEMENT INTEGRATING LOW COST GFRP FITTINGS AND MEMBERS

1980 - DESIGN OF GFRP 4.6-METER CUBE
- FABRICATION OF ALL COMPONENTS

1981 - ASSEMBLY AND TEST OF 4.6-METER CUBE

1982 - MESH MODEL FABRICATION AND TEST
- ASSEMBLY AND TEST OF GATE FRAME TRUSS

1983 - METAL MATRIX COMPONENT DESIGN, FABRICATION, TEST
- PRECISION JOINT DESIGN, FABRICATION, TEST

Figure 2

HISTORY OF THE BOX TRUSS (CONCLUDED)

1984 - METAL MATRIX COMPONENT DESIGN, FABRICATION, TEST
- MESH TIE SYSTEM ANALYTICAL DEVELOPMENT
- PASSIVE DAMPING COMPONENT DEVELOPMENT

1985 - FABRICATION OF 4.5 METER BOX TRUSS ANTENNA
- DYNAMIC TEST OF STATICALLY DETERMINATE AND INDETERMINATE TRUSSES

1986 - TESTING OF 4.5 METER BOX TRUSS ANTENNA

BOX TRUSS ANTENNA MODEL

A model of a box truss mesh antenna is shown in Figure 3. Mesh support posts (standoffs) separate the radiating surface from the support structural. This separation provides the volume necessary to stow the mesh and mesh tie system and assures that neither the mesh nor the tie cords impinge on the deployment of the box truss. Generally, the standoffs are tubes of similar cross section to the box truss vertical members and are inserted into the corner fittings. The mesh is attached to the top of the standoffs. The vertical members on the box truss structure are vertical rather than perpendicular to the surface to assure step-by-step deployment and stowability.

To achieve the parabolic curve shape, each box truss face consisting of two vertical members and two surface tubes is sheared by using different length interior diagonal members.

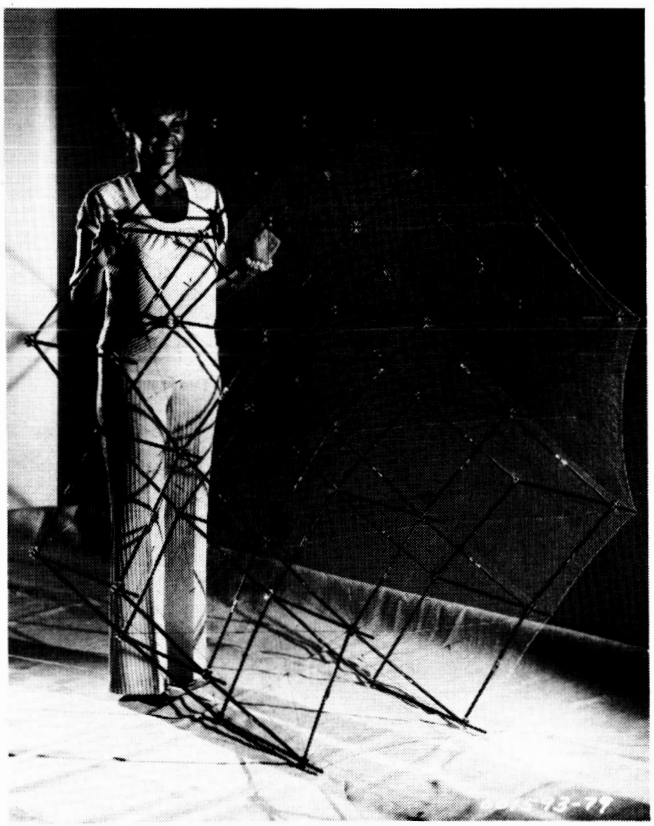

Figure 3

FULL-SCALE PROTOTYPE CUBE

During 1980, the design of each of the box truss components was reviewed and redesigned to achieve optimize weight, cost and thermal stability while meeting the stowed, deploying and deployed structure requirements. A prototype was made for each component and tested to verify manufacturing methods (feasibility and tolerance manageability) stiffness, strength, and weight. By the end of 1980, all components for a full-scale prototype 4.5-meter, deployable box truss cube were completed and assembly had started. Final assembly was completed in 1981. Summarized below are the design features of the full-scale prototype cube. Figure 4 shows the resulting prototype cube in a deployed configuration

4.5m Deployable Cube
Stows in 0.3m square by 4.5m long (0.15m per module)
36 modules (28m x 28m deployed) stows in 1m by 1m by 4.6m
All GFRP except for hinge pins and springs
High performance (high stiffness, low CTE)
Low Weight - 27 kg
High Accuracy - better than 0.1mm on all axes
All components and members fully constrained when stowed
Corner fitting stabilized by bonded interface to vertical

A 4.5-meter diameter mesh reflector has now been integrated to the box truss cube.

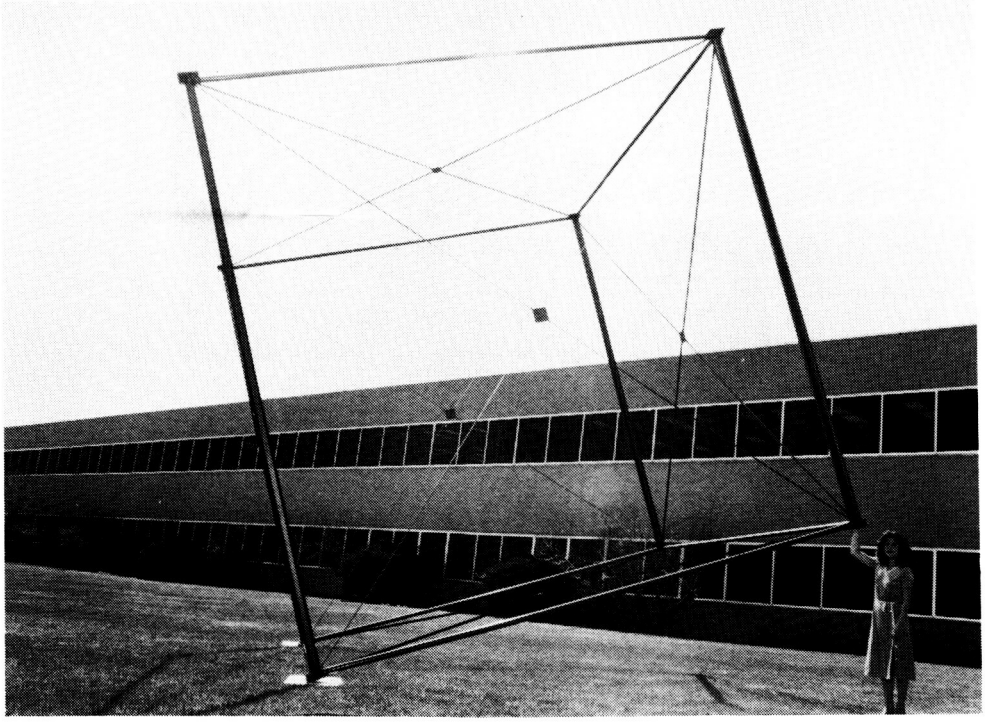

Figure 4

ANALYSIS OF BOX TRUSS MESH ANTENNAS

An integrated system has been developed to model, analyze, and predict rf performance of box truss antennas with reflective mesh surfaces. This analysis system is unique in that it integrates custom-written programs for cord-tied mesh surfaces, thereby drastically reducing both the man-hours and computer-dollars required to design and analyze mesh antennas. The program can be used to analyze the effects of (1) on-orbit thermal environments, (2) solar pressure, (3) on-orbit calibration or continuous adjustment of the mesh tie system to improve surface accuracy, and (4) gravity distortions during setting.

The analysis system uses nonlinear finite-element, surface topography and interpolation, and rf aperture integration techniques. The system provides a quick and cost-effective final link in the design process for box truss antennas. (Fig. 5.)

- PROGRAM CAN BE USED TO ANALYZE EFFECTS OF:
  - ON-ORBIT THERMAL ENVIRONMENTS
  - SOLAR PRESSURE
  - ON-ORBIT CALIBRATION OR CONTINUOUS ADJUSTMENT OF MESH TIE SYSTEM TO IMPROVE SURFACE ACCURACY
  - GRAVITY DISTORTIONS DURING SETTING
  - MANUFACTURING ERRORS
- PROGRAM USES:
  - NON-LINEAR FINITE ELEMENT
  - SURFACE TOPOGRAPHY AND INTERPOLATION
  - RF APERTURE INTEGRATION
- PROGRAM CONSISTS OF SIX CUSTOM WRITTEN INTEGRATED PROGRAMS

Figure 5

TYPICAL BOX TRUSS ANTENNA AND MESH TIE SYSTEM

Figure 6 shows that the direct tieback tie system consists of three types of cords: the surface cross cords that bisect the mesh reflective surface, the surface radial cords that extend radially from the top of the standoffs to the surface cross cords, and the tieback cords that extend from the surface cords to the bottom of the standoffs. The bottom of the standoffs correspond to the location of the corner fittings and the box truss. The tieback cords pull the surface into shape and are tied along each surface cord at a distance defined as the radial tie spacing.

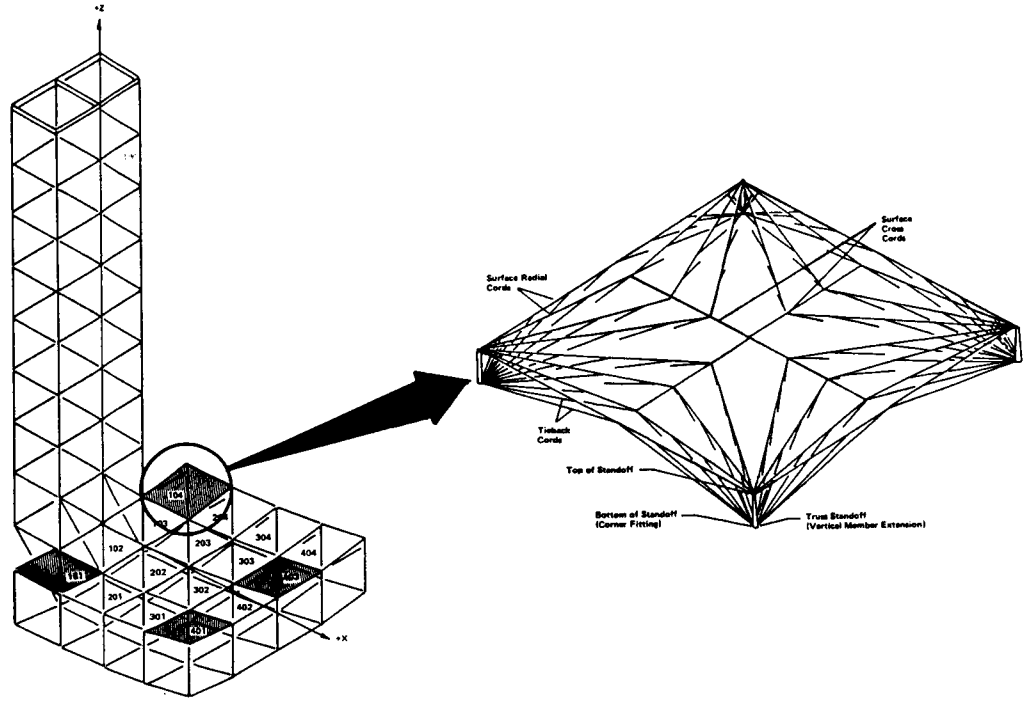

Figure 6

INTEGRATED MESH ANALYSIS SYSTEM

The complete analysis system consists of six integrated computer programs (Figure 7).

1) Mesh Tie System Generator: creates the tie system design and finite-element model of the tie system.
2) Loadcase Generator: creates the loadcases to be placed on the tie system finite-element model. These loadcases can represent any operational or manufacturing environment.
3) Model Optimizer: generates the optimized finite-element input file for the model solver.
4) Model Solver: determines the tie system distortions by solving the tie system finite-element model for the above specified loadcases.
5) Antenna Surface Topography Solver: determines the best-fit paraboloidal surface, effective feed scan, axial defocus, and minimum rms surface error to match surface distortions.
6) RF Performance Solver: determines the far-field pattern, antenna gain, and beam efficiency of the antenna.

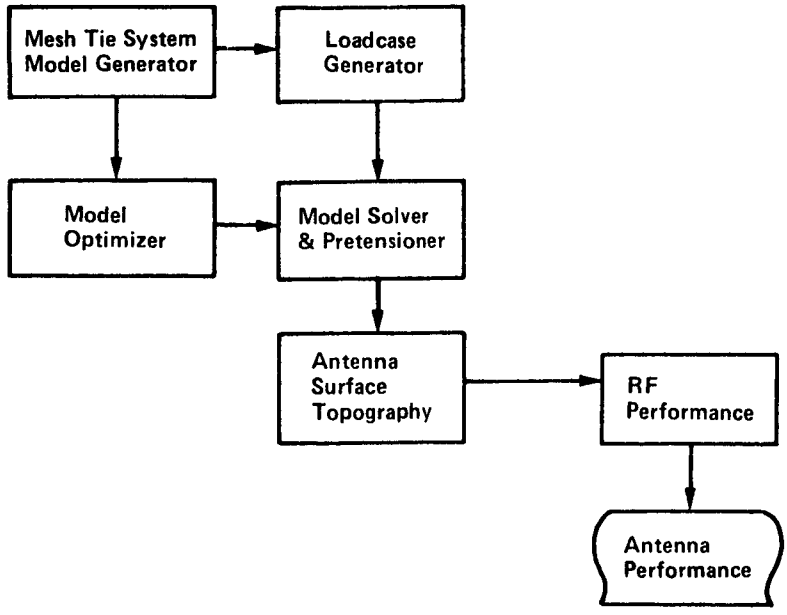

Figure 7

PROGRAM INPUTS AND OUTPUTS

Figure 8 describes the user inputs and program outputs for each program. Illustrated is the fact that the Mesh Tie System Model Generator and the Loadcase Generator programs are used to define all inputs necessary for analyzing a mesh reflector. This allows the larger, more time consuming programs, e.g., the Model Solver, to be run in a batch mode thereby reducing run costs. In the example shown in Figure 8, effects due to tie cord temperatures and g-loading are being analyzed via the Loadcase Generator. Other options allow point loads and pressures to be analyzed.

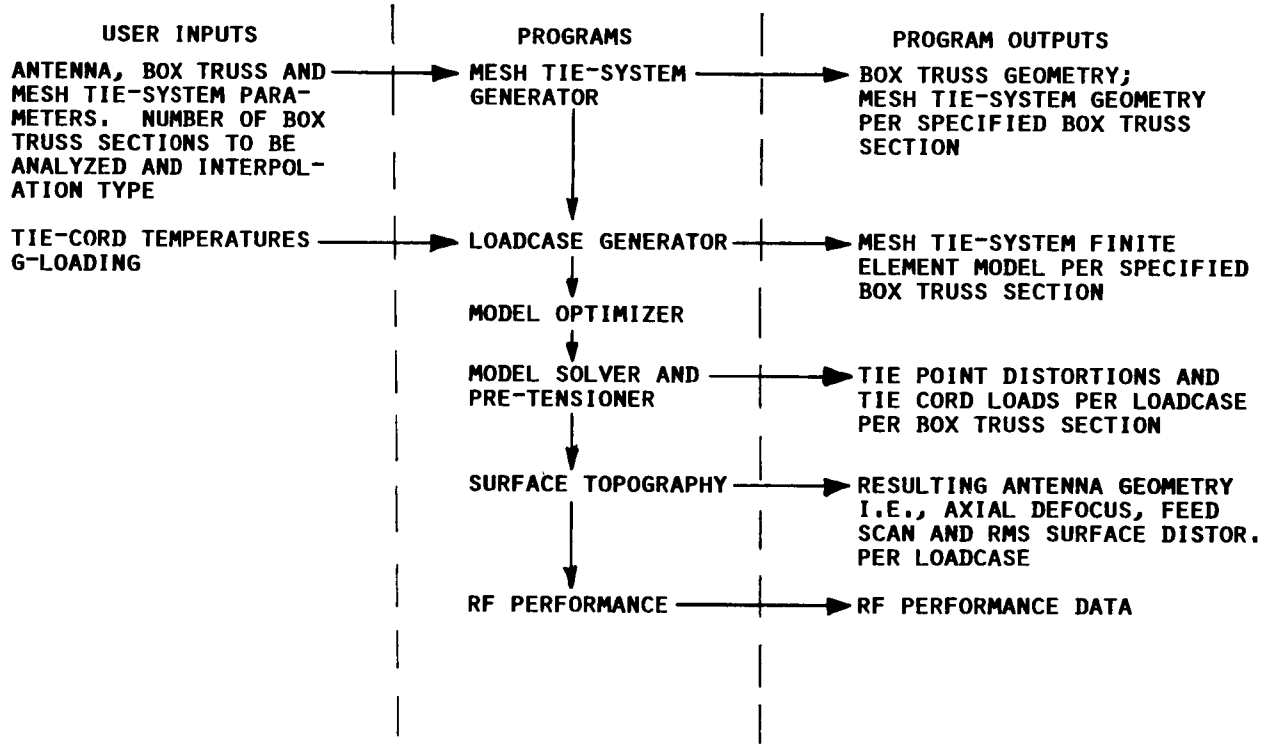

Figure 8

DYNAMIC TESTING OF BOX TRUSS STRUCTURE

Testing was performed to quantify the effects of joint freeplay on a multi-bay statically determinate truss, and then assess the effects when the structure was modified to incorporate pretensioned diagonals producing a statically indeterminate truss. Also evaluated were the effects of levels of dynamic load on the dynamic performance of the truss. Testing of four truss configurations was performed:

1) Truss with tight joints.
2) Truss with joints having normal freeplay.
3) Truss with joints having excessive freeplay (3 times or more than normal freeplay).
4) Truss with normal freeplay and cross-tensioned diagonals.

The effect of magnitude of dynamic load was assessed for each test.

0 OBJECTIVE:

- UNDERSTAND EFFECTS OF JOINT FREEPLAY ON DYNAMIC TRUSS BEHAVIOR

0 APPROACH:

- BUILD AND TEST 2M x 20M 10-BAY TRUSS WITH NO FREEPLAY, 1 MIL FREEPLAY AND 3 MIL FREEPLAY. ALSO TEST CROSS-TENSION DIAGONALS.

Figure 9

DYNAMIC TEST ARTICLE

A test article for this purpose was designed and built. The test article consisted of ten bays of planar truss, each measuring 2-meters per side, suspended by long wires at each joint. Each side was made of square aluminum tubing, and all corner fittings were made of cast aluminum. Pins of varying size were used to assemble the truss thereby simulating various joint freeplay conditions. All joints could be shimmed and bolted tight to assure a no freeplay condition. Single, unloaded tube diagonals were interchangeable with dual, pretensioned steel rod diagonals. Modal analyses of the suspended tube diagonal configuration were conducted and used to calculate frequency response functions simulating proposed test conditions for the purpose of evaluating the suspension system. Figure 10 shows the test article with the pretensioned steel rod diagonals installed.

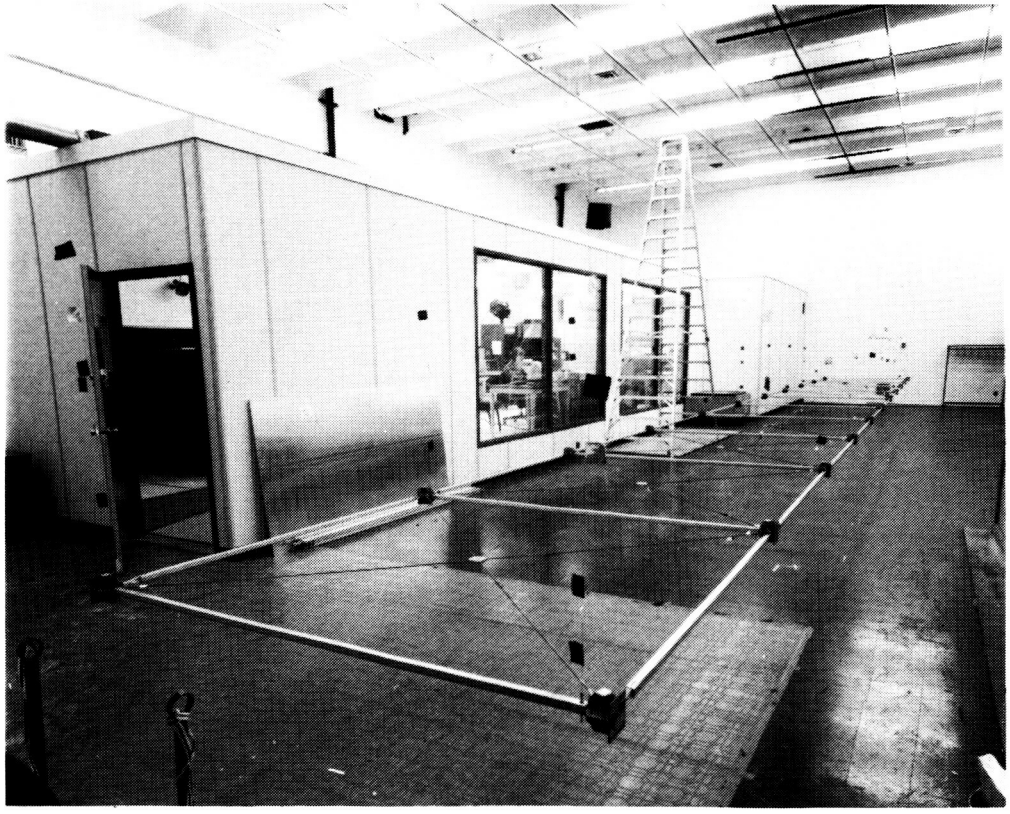

Figure 10

GENERAL TRENDS

General trends were observed for the various test models relative to the zero freeplay test model. At 1-mil freeplay both a small decrease in frequency and an increase in damping were observed. At low-level force input the structure did exhibit some nonlinear behavior. At high-level force input the structure behaved as a linear structure.

However, at 3-mil freeplay the structure was extremely nonlinear regardless of the force level. It also exhibited high damping which would be expected in a very sloppy structure. (Fig. 11.)

- 1 MIL FREEPLAY
  - DECREASES FREQUENCY
  - INCREASES DAMPING
  - LINEAR STRUCTURE AT HIGHER INPUT
  - NON-LINEAR RESPONSE AT LOWER INPUTS
- 3 MIL FREEPLAY
  - EXTREME NON-LINEAR RESPONSE
  - HIGH DAMPING

Figure 11

2-METER TRUSS DYNAMIC TEST RESULTS

The existence of local pinned-pinned bending frequencies of the 2-meter truss member in the range of global truss bending frequencies caused the introduction of a multitude of local/global bending modes. Because the shape and frequency of such modes depend on unknown and nonlinear effects, such as joint fixity and local bending frequency variations due to oscillating loads in global modes, exact analytical predictions were difficult.

Quantification of the effect of joint freeplay was met. The tube diagonal configuration test data provided the information for this objective. The 1-mil freeplay resulted in a drop in frequency. (First global truss bending mode was identified at 20 Hz without freeplay and at 17.72 Hz with freeplay.) This frequency shift was consistent with that predicted by the Martin Marietta Denver Aerospace developed "Modal Freeplay" method, indicating that this method could be applied in future large space structures.

Damping is the least accurate parameter identified by curve fitting test transfer functions. Therefore, the uncertainties of the identified mode shapes and frequencies were of such magnitude as to preclude any exact definition of the effect of freeplay or preload on modal damping. (Fig. 12.)

- THE TEST ARTICLE EXHIBITED A MULTITUDE OF LOCAL/GLOBAL COUPLING MODES.
- INSTRUMENTATION WAS INSUFFICIENT TO IDENTIFY ALL MODES.
- LOCAL/GLOBAL COUPLING PREVENTED THEORETICAL/EXPERIMENTAL CORRELATION IMPROVEMENT OF MODES THAT WERE IDENTIFIED.
- SUFFICIENT DATA WERE OBTAINED TO EVALUATE THE MODAL FREEPLAY METHODOLOGY.
- ASSESSMENT OF THE EFFECTS OF PRETENSIONED DIAGONALS WAS IMPEDED BY LOCAL/GLOBAL COUPLING EFFECTS.
- QUALITY OF TEST DATA DID NOT ALLOW IDENTIFICATION OF RELIABLE MODAL DAMPING VALUE.

Figure 12

FABRICATION OF 4.5-METER BOX TRUSS ANTENNA

A 4.5-meter diameter offset mesh reflector was fabricated and integrated to an all graphite epoxy box truss cube. The reflector surface was designed to operate at X-Band (10 GHz) with a surface accuracy of 1/20 of a wavelength. Three objectives were achieved during the fabrication, setting and measurement of the antenna. These objectives were to: 1) demonstrate the fabrication methods for both mesh and tie system, 2) demonstrate performance of modular tie system to precisely position and hold mesh surface, and 3) verify empirical relationships for predicting rms surface errors due to mesh pillowing and manufacturing tolerances. (Fig. 13.)

0 OBJECTIVES:

- DEMONSTRATE FABRICATION METHODS FOR MESH AND TIE SYSTEM
- DEMONSTRATE MODULAR TIE SYSTEM
- CHARACTERIZE PILLOW SHAPES

0 APPROACH:

- BUILD 4.5 METER DIAMETER OFFSET MESH REFLECTOR INTEGRATED TO THE ALL GRAPHITE EPOXY BOX TRUSS DESIGNED TO OPERATE AT X-BAND

Figure 13

DIRECT TIEBACK TIE SYSTEM FEATURES

The depth of the mesh tie system can be optimized to produce either minimum packaging or maximum stability (thermal and structural). Also, the tie system cords do not span the entire width of the box section. This feature enables the tie system of each box section to be manufactured separately. This also helps to eliminate interaction between the tie systems of adjacent box sections, allowing each tie system of each box to operate independently. Consequently this produces a more stable reflector surface because local environmental effects such as shadowing of a single box section will not affect the precision of other box sections. Because each tie system operates independently, analysis and testing of the complete reflective surface can be performed on a per box section basis. (Fig. 14.)

- THE MESH IS ATTACHED TO STANDOFFS WHICH CAN BE DESIGNED FOR MINIMUM THERMOELASTIC DISTORTION OF REFLECTOR (LONGER STANDOFFS) OR MINIMUM PACKAGING VOLUME (SHORTER STANDOFFS)
- CONTINUOUS MESH SURFACE IS MADE BY SEWING THE INDIVIDUAL BOX SECTION MESH PANELS TOGETHER
- EACH INDIVIDUAL BOX SECTION MESH TIE SYSTEM IS MODULAR (INDEPENDENT OF ADJACENT BOX MESH TIE SYSTEMS)
- TIE SYSTEM MODULARITY FEATURE SIMPLIFIES MANUFACTURING AND SETTING OF ANTENNA. NO MATTER HOW LARGE THE ANTENNA, INDIVIDUAL BOX SECTIONS (MUCH SMALLER $\approx$ 3-10 M) CAN BE SET INDEPENDENTLY
- TIE SYSTEM MODULARITY IMPROVES OPERATIONAL STABILITY BY ISOLATING LOCAL EFFECTS (EG. SHADOWING)

Figure 14

MESH AND TIE SYSTEM PRIOR TO SETTING

Integration of the reflector onto the box truss was completed in two main steps. First the mesh and tie system were installed onto the standoffs and the surface coarsely set to shape while the standoffs were installed in ground level wooden stands. Then, the standoffs and reflector were installed onto the box truss and the fine surface adjustment was completed. This two step process was used so no major scaffolding was needed to either mate the tie cord system to the mesh or set the surface to the paraboloidal shape. Figure 15 shows the reflector surface immediately after the tie system had been mated to the mesh and installed on the standoffs.

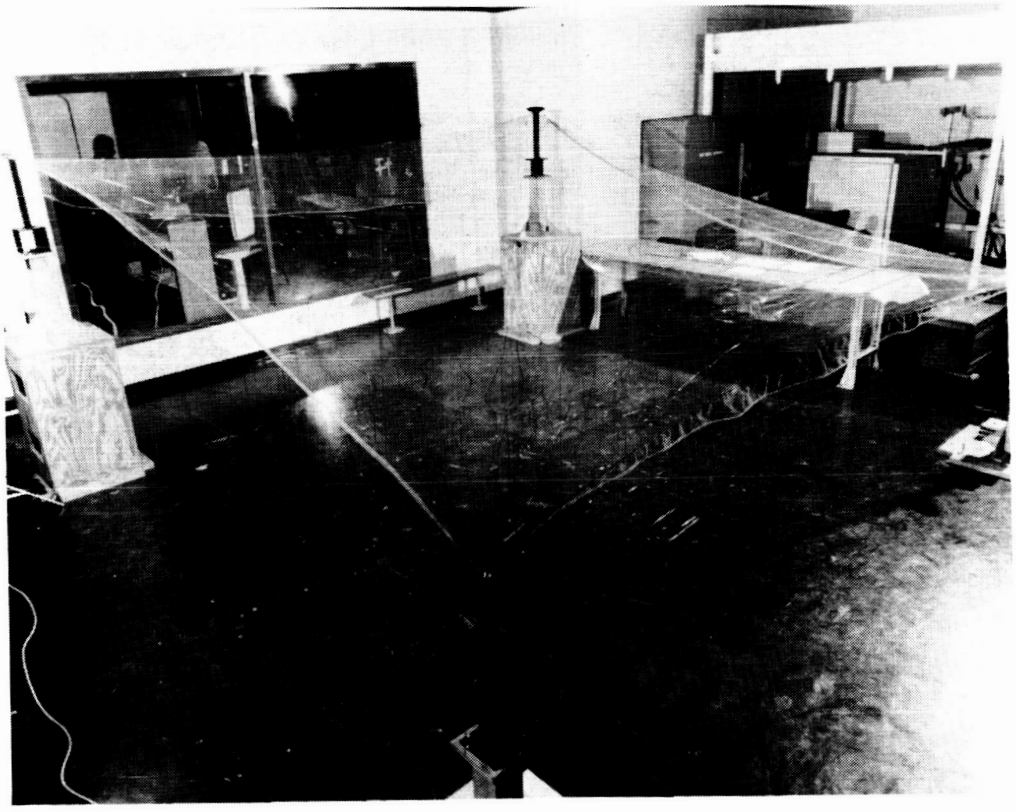

Figure 15

MESH TIE SYSTEM DURING SETTING

Figure 16 shows the next assembly step of the mesh reflector. Each tieback cord was inserted into the adjustment fittings and the surface was coarsely adjusted to shape. The adjustment fittings are an integral part of the standoff. Also shown in Figure 16 is the fact that each radial surface cord has been tensioned by attaching a weight to the end of the cord and hanging the weight over the top of the standoff. The weight is free to move thereby applying a constant tension of the surface cords. The amount of weight (1/4 lb per cord) was based on the relationship between surface cord tension, bi-axially tensioned mesh and the maximum allowed rms surface error due to mesh pillowing.

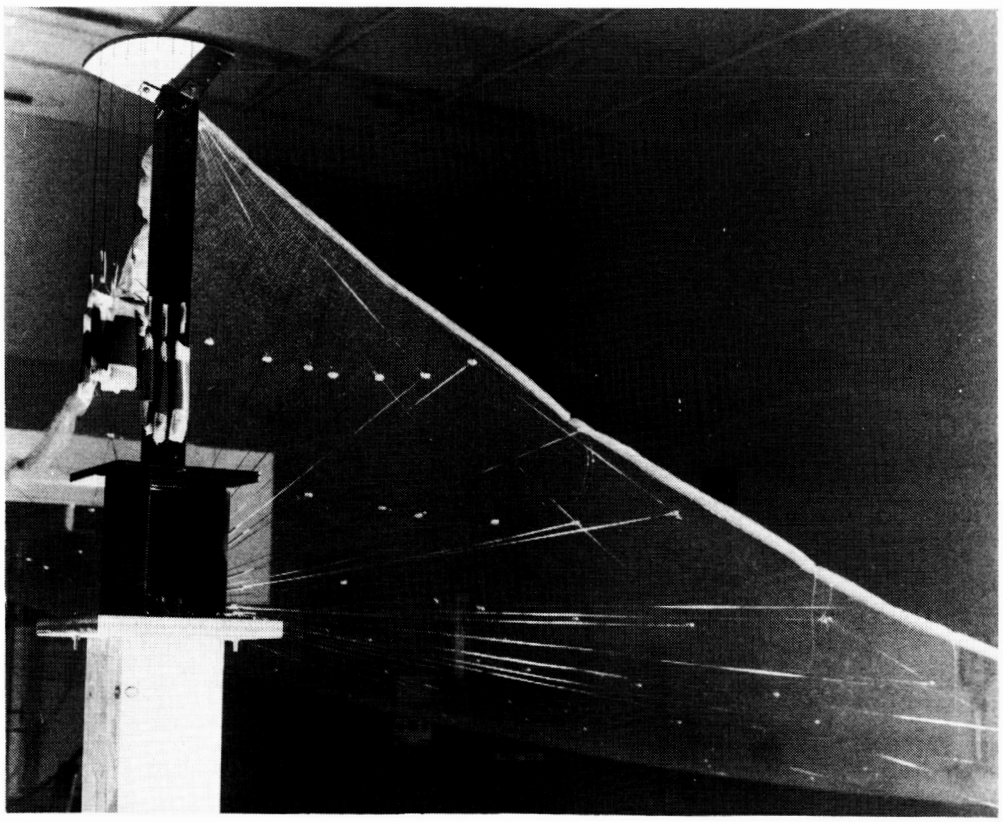

Figure 16

COMPLETED 4.5 METER ANTENNA

Figure 17 shows the completed 4.5-meter mesh reflector installed on the box truss just prior to having the surface verified by metric camera measurements. Although the box truss is rigid enough to be set upright, the metric camera measurements required the reflective surface to be parallel to the floor.

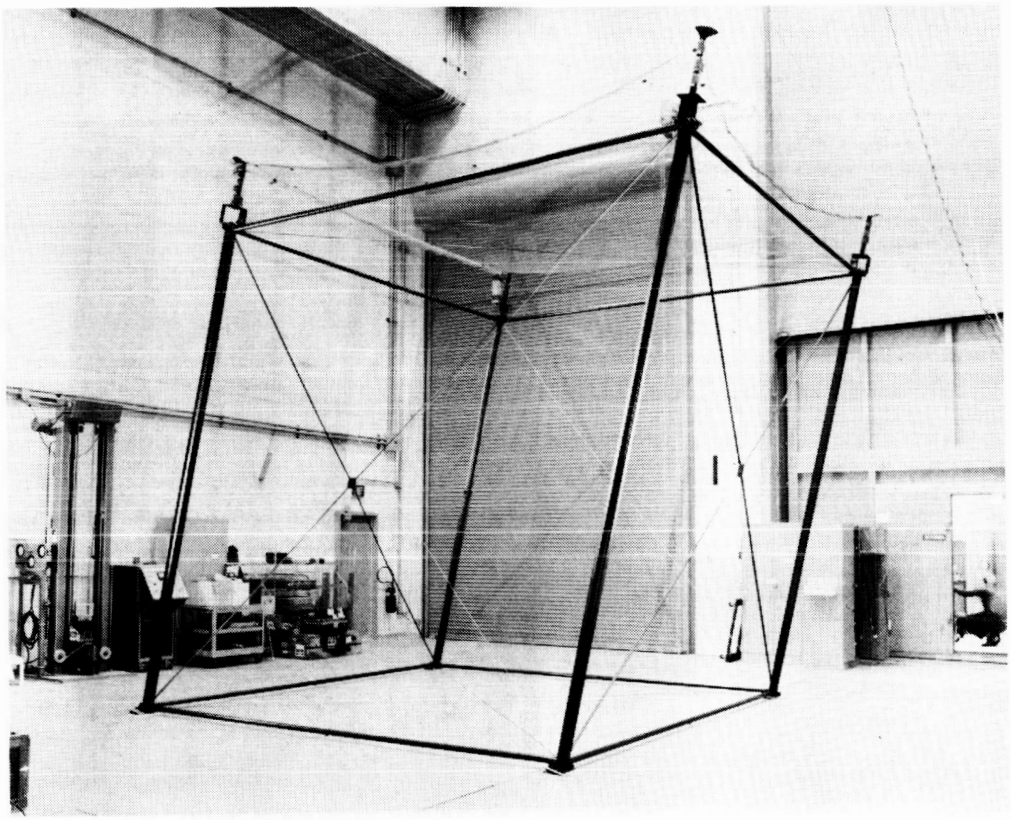

Figure 17

MEASUREMENT RESULTS FOR THE 4.5 METER ANTENNA

Figure 18 summarizes the surface verification results for the reflector. The results were obtained by using the metric camera measurements of the 176 tie points and 40 special mesh targets. The coordinates of 176 tie points were then used in a 'best-fit' analysis to determine the rms manufacturing error. The coordinates of the 40 mesh targets were used to determine the rms surface error due to mesh pillowing.

To determine the repeatability of the reflector two sets of surface measurements were performed. Set 1 was completed immediately following the theodolite surface setting. Set 2 was completed after the reflector had been partially stowed and redeployed.

In addition, during the 'best-fit' analysis, we found that one particular area of the reflector had been set lower than the rest of the surface due to improper initialization of the theodolite system. Therefore, the 'best-fit' analysis was completed for both the whole surface and the part of the surface that was unaffected by the improper initialization procedure.

	Whole Surface/ Set 1	Partial Surface/ Set 1	Whole Surface/ Set 2	Partial Surface/ Set 2
RMS Manufacturing Error, in	0.050	0.040	0.049	0.041
RMS Pillowing Error (ave), in	0.026	0.026	0.026	0.026
Worst - Case Sum, in	0.076	0.066	0.075	0.067
RSS of RMS Errors,	0.056	0.048	0.055	0.049
Average of Worst - case/RSS, in	0.066*	0.057**	0.065Δ	0.058ΔΔ

* - represents surface accuracy of 1/18 of a wavelength

** - represents surface accuracy of 1/21 of a wavelength

Δ - represents surface accuracy of 1/18 of a wavelength

ΔΔ - represents surface accuracy of 1/20 of a wavelength

Figure 18